

EFFECTS OF COMBUSTION SYNTHESIS PROCESSING AND PARTICLE SIZE ON $(Y_{1-m-n}Ce_mGd_n)_2SiO_5$ PHOSPHOR

E. J. Bosze, J. McKittrick, G.A. Hirata and L. E. Shea*

University of California at San Diego, Department of Mechanical and Aerospace Engineering and Materials Science Program, 9500 Gilman Drive, La Jolla, CA 92093-0411 ebosze@ucsd.edu

*Sandia National Laboratory, P.O Box 5800, Albuquerque, NM, 87185-0527

ABSTRACT

The blue-emitting phosphor, yttrium silicate activated with cerium $(Y_{1-m}Ce_m)_2SiO_5$, was produced by combustion synthesis. The effect of particle size and processing conditions on the cathodoluminescence efficiency was investigated. Thermodynamic modeling of the combustion reaction shows that as the fuel-to-oxidizer ratio increased, the amount of gases produced by the reaction also increased. X-ray diffraction and transmission electron microscope micrographs show an increase in the crystallite size with increasing fuel amount. Powders annealed at 1350°C for 1 hour were settled in deionized H₂O and attrition milled to determine the effect of particle size on the efficiency. The efficiency of the settled powders was not found to be dependent on the particle size. The efficiency of the milled powders decreased with increasing milling time.

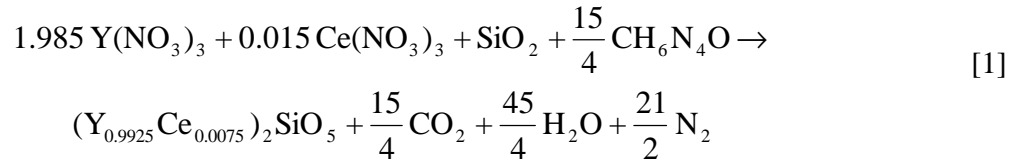
INTRODUCTION

Flat panel displays, such as plasma displays panels (PDP's) and liquid crystal displays (LCD's), are emerging as replacements for the heavy and bulky cathode ray-tube displays (CRT's) that dominate the TV and computer monitor markets. The success of the CRT is due to the ability of these displays to produce a bright image with a large viewing angle with a wide range of colors (or large color gamut). Problems with LCD's and PDP's range from a small viewing angle (~ 45°) and problems with displaying moving objects for LCD's to the high cost of production for both LCD's and PDP's (1).

A promising flat panel display, the field emission display (FED), is currently under development and in limited production. FED's are the next generation cathodoluminescent display. Both CRT and FED technologies use electron bombard of phosphors to produce light (cathodoluminescence). FED's consist of a phosphor coated screen separated ~ 2.5 mm by spacers from a field emitter array (FEA). FEA's have millions of inverted cone shaped cold cathode electron emitter tips, up to 10⁷ emitters/cm² (2). These emitter tips emit electrons and are then accelerated with a potential lower than CRT's, varying from 0.2 to 10 keV as compared to 20 to 30 keV for CRT's. Thousands of emitters are able to bombard the red, green or blue emitting phosphors. Due to the lower acceleration voltages, the FED screen is not as bright as that of the CRT. To improve the brightness of FED's, phosphors with high efficiencies at low acceleration voltages are currently being investigated.

The resolution of the screen is determined by the pixel size. To produce a higher resolution display, the phosphor particle size must be small enough for several particles to be contained within one red, green or blue emitting subpixel. It has been shown in several studies that as the particle size decreases, the luminescence intensity also decreases (3, 4). Phosphors are thought to have a 'dead layer', which extends from the surface to some distance inside the particle (4). This dead layer is the region where the probability of luminescence is less than for the rest of the particle. As the particle size decreases, the ratio of the dead layer to the particle size diameter increases leading to a decrease in the luminescent intensity (4). McKittrick et. al (3) reported that as the particle size increases, the luminescence emission intensity increases due to the reduction of the surface defects and absorbed species that could quench the luminescence. As the particles are annealed at high temperatures, the crystalline size increases and these defects are annealed out of the particles.

The blue emitting phosphor yttrium silicate activated with Ce^{3+} , $(Y_{1-m}Ce_m)_2SiO_5$, is being investigated as a potential phosphor for FED's. To increase the efficiency of this phosphor, Y^{3+} is replaced with Gd^{3+} which acts as a sensitizer for Ce^{3+} , $(Y_{1-m-n}Ce_mGd_n)_2SiO_5$, by transferring energy to Ce^{3+} . The optimum concentrations were found to be $m=0.0075$ and $n=0.15$ (5). Powders were produced by an oxide synthesis technique called combustion synthesis (6). The stoichiometric combustion reaction that forms $(Y_{0.9925}Ce_{0.0075})_2SiO_5$ from metal nitrates and SiO_2 powders with the fuel carbohydrazide (CH_6N_4O) is:



The combustion synthesis reaction can be controlled by varying the fuel-to-oxidizer ratio (f/o), which is the ratio of the number of moles of carbohydrazide to the number of moles of yttrium nitrate ($Y(NO_3)_3$), cerium nitrate ($Ce(NO_3)_3$) and SiO_2 . Particles in the as-synthesized condition were found to be very porous, had plate-like particles, and exhibited the low temperature (X_1) phase of Y_2SiO_5 . Annealing at $1350^\circ C$ for 1 hour transformed the X_1 phase into the more luminescent X_2 phase. The crystallites grew and become round however sintering was also taking place, forming large agglomerates.

The purpose of this study was to determine the effect of particle size on the luminescence intensity of this phosphor. Powders were milled with an attrition mill and settled for different times. Other powders were produced with varying f/o ratios to determine how the escaping reaction gases influence the size and porosity of the particles and the crystallite size.

EXPERIMENTAL

Yttrium silicate activated with the optimum concentrations of Ce^{3+} and Gd^{3+} $(Y_{1-m-n}Ce_mGd_n)_2SiO_5$ were produced by combustion synthesis with carbohydrazide fuel. Details on the combustion synthesis reaction for this phosphor can be found in (5, 7). Table I lists the f/o ratios studied.

Table I. Fuel-to-oxidizer ratios.

f/o ratio	percent fuel rich or lean
0.885	30% fuel lean
1.250	Stoichiometric
1.615	30% fuel rich
2.012	60% fuel rich

X-ray diffraction (XRD) was performed on the powders to determine the crystallite sizes and transmission electron microscopy (TEM) was performed to directly determine the crystallite size and porosity. The crystallite size from XRD data was determined using the Scherrer formula (8):

$$t = \frac{0.9\lambda}{B \cos(\theta)} \quad [2]$$

where t is the crystallite size (nm), B ($B = \sqrt{B_m^2 - B_s^2}$) is the broadening (measured in radians at the full width at half maximum for several peaks) and $\lambda = 0.154$ nm (CuK $_{\alpha}$ radiation). XRD scans were taken in the 2θ mode at $1^\circ/\text{min}$ from 20 to 45° . The system broadening was found to be $B_s = 5.36 \times 10^{-4}$ radians using a polycrystalline silicon standard. TEM images were taken with a Philips CM30, with 300 keV beam. Thermodynamic modeling of the combustion synthesis reaction was done using TEQWORKS (9) to determine the composition and mass fraction of the gases that are produced from the reaction.

A portion of the as-synthesized powders were annealed at 1350°C for one hour before settling and milling from 1 to 24 hours using ZrO $_2$ ceramic media. A 75%/25% 2-propanol/deionized water mixture was used as the milling dispersion liquid. Powders were settled by dispersing the powder in a solution of deionized water adjusted to a pH of ~ 4 with HCl. The powder was first ultrasonicated for 1 hour and then allowed to settle for different times: 1, 15, 30, 60, 120, 240 minutes. The predicted size of the particles was calculated by using the following sedimentation equation derived from Stoke's Law (10):

$$d^2 = \frac{18\eta h}{t(\rho - \rho_o)g} \quad [3]$$

where d is the particle diameter (m), η is the dispersant viscosity of water (8.9×10^{-4} kg/m-s), t is the sedimentation time (sec), ρ is the density of the powder (4441 kg/m 3), ρ_o is the density of the water (1000 kg/m 3), g is the acceleration due to gravity (9.81 m/s 2) and h is the settling height (0.083 m). Particle size was determined by a Horiba LA-300 laser scattering particle size analyzer. The cathodoluminescence (CL) efficiency of the settled and milled powders were measured with the following electron excitation energies; 1, 3, 5 and 7 keV.

RESULTS AND DISCUSSION

Yttrium silicate exhibits two monoclinic phases: X_1 is the low temperature phase with a $P2_1/c$ space group and has a transition temperature of $\sim 1050^\circ\text{C}$ to the X_2 high temperature phase with a $C2/c$ space group (7). The X_2 phase material has been found in previous studies to have a higher luminescent efficiency and better chromaticity coordinates (7, 11). Figure 1 shows XRD scans for as-synthesized powders produced with different f/o ratios. For a f/o = 0.885 (30% fuel lean), the powders were found to have the smallest crystallite size as indicated by the broad XRD peaks. The crystallite size was found to increase with increasing f/o ratio, with the largest crystallite size found for f/o = 2.012 (60% fuel rich). Table II shows results from XRD line broadening analysis using Eq. [2] and the identification of the phases present. It is believed that as the amount of fuel is increased, the reaction temperature also increased, facilitating crystal growth.

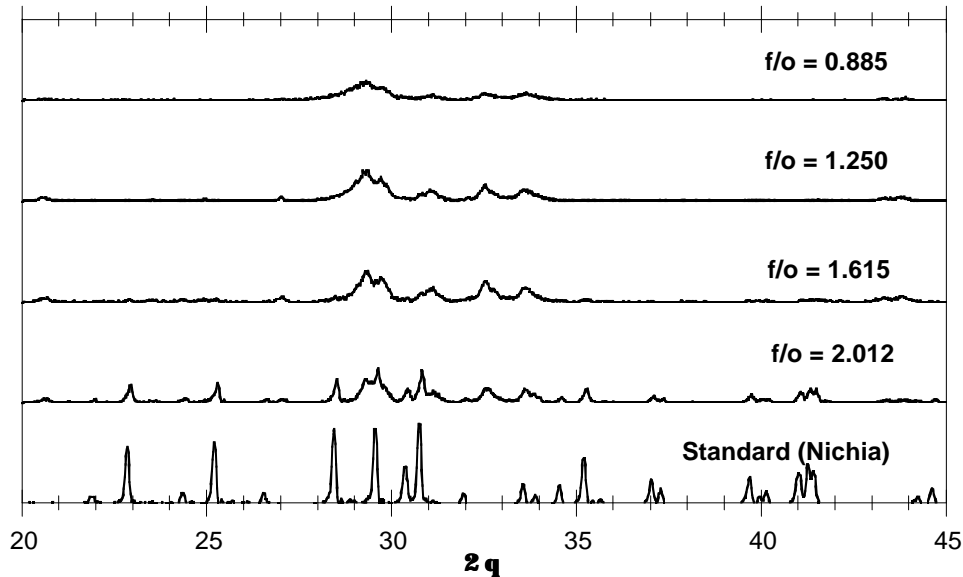


Figure 1. XRD scans of as-synthesized powders made with different fuel/oxidizer ratios.

Table II. Calculated crystallite size calculated using line broadening analysis along with phases. * JCPDS #41-4, [§] JCPDS #36-1476.

Amount of Fuel	f/o ratio	Crystallite Size (nm)	Phase
30% Fuel Lean	0.885	31	X_1^*
Stoichiometric	1.25	44	X_1
30% Fuel Rich	1.615	56	X_1
60% Fuel Rich	2.012	110	X_1 & X_2^{\S}
Standard	--	172	X_2

Figure 3 shows the results from the thermodynamic modeling of the predicted mass fraction of the gases and the amount of solid product produced for each of the f/o ratios. Analysis shows that as the amount of fuel is increased, the number of moles of gas also increased, in particular N_2 . Figure 4 plots the total mass fraction of gas showing a linear increase in the total amount of gas as the fuel amount is increased. Figure 4 suggests that as the amount of gas increases, the more likely the hot escaping gases will break up agglomerates and more porosity would be observed.

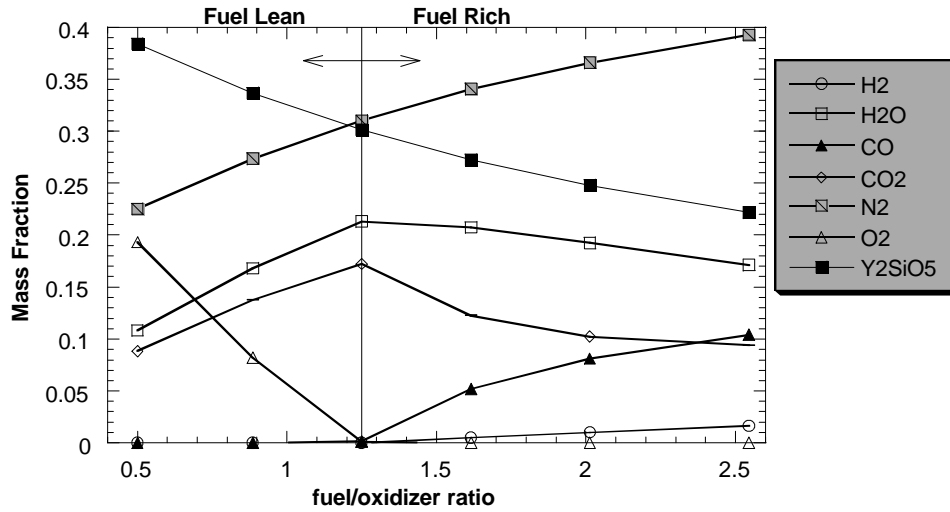


Figure 3. Thermodynamic modeling of the combustion reaction showing the mass fractions of products formed with various f/o ratios.

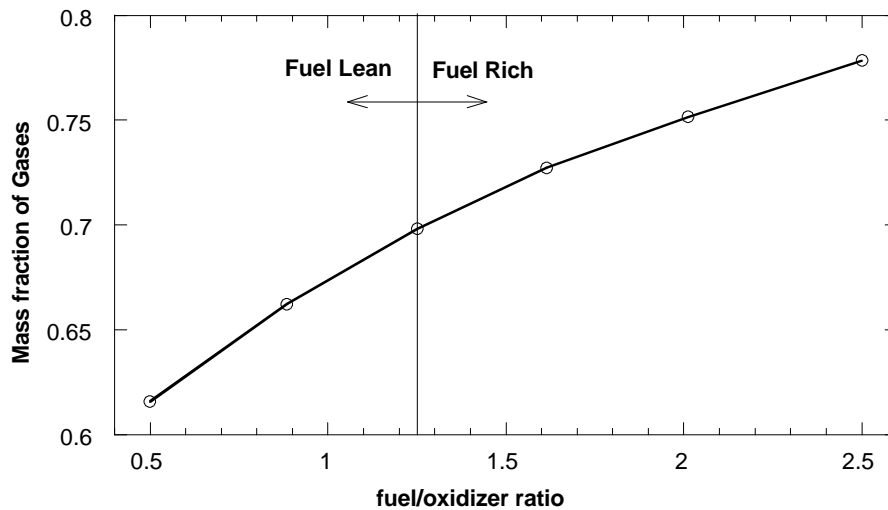


Figure 4. Mass fraction of gas produced as a function of f/o ratio during the combustion synthesis reaction.

Figure 5 shows the particle size distribution of the as-synthesized powders for each f/o ratios. Table III shows the mean diameter of the particles measured by laser

scattering and the coefficient of variation (CV), which is a measure of the broadness of the particle size distribution. Figure 5 reveals that the particle size is not affected by the f/o ratio, even though the amount of gases produced by the reaction increases with an increase in f/o ratio. Table III shows that the standard has the narrowest distribution of particles while the combustion synthesized powders have an average coefficient of variation of 52%, 20% wider than that of the standard.

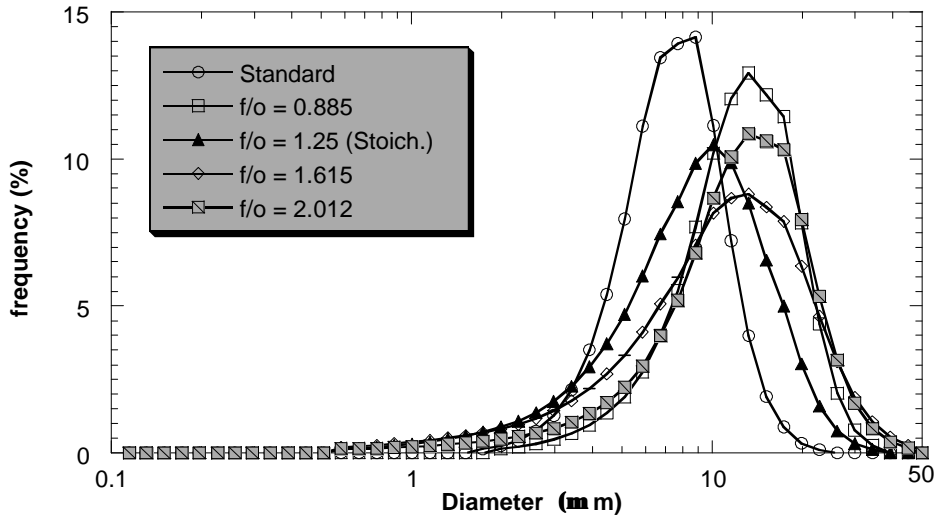


Figure 5. Particle size distribution of as-synthesized particles compared with a standard (Nichia).

Table III. The mean diameter particle size and the coefficient of variation (CV) for various fuel/oxidizer ratios.

fuel/oxidizer ratio	Mean Diameter Particle Size (μm)	CV (%)
0.885	12.3 ± 5.1	41.1
1.250 (Stoich.)	9.0 ± 4.9	53.9
1.615	11.5 ± 7.1	61.5
2.012	12.5 ± 6.4	51.3
Standard	7.3 ± 2.8	38.2

Figure 6 (a) is a bright field TEM micrograph from powders formed in f/o = 2.012 (60% fuel rich) powders, with the inset showing the diffraction pattern from these particles. Figure 6 (b) is a bright field image from powders from the f/o = 2.012, with the inset showing the diffraction pattern of this particle. Figure 6 (a) shows a particle made up of large, faceted crystallites while the particle in 6 (b) exhibits a "foamy" structure made up of much smaller crystallites. This is more clearly shown in dark field images shown in Figure 7 (a) and (b). Figure 7 (a) was formed by displacing the objective aperture around the spots just outside the main beam. In Figure 7 (b), the objective aperture was displaced to the first bright ring to form this image. This reveals the small crystallites that make up the "foamy" structure of this particle. Analysis of the diffraction pattern in Figure 6 (a) and (b) show that the rings in 6 (b) conform to the low temperature X₁ phase of this material while the spots in 6 (a) conform to the high temperature X₂ phase. TEM images of particles from batches with f/o < 2.012 show particles that exhibit

the "foamy" structure shown in Figure 6 (b), with crystallite sizes that decrease as the f/o ratio decreases, thus confirming the results obtained from the XRD. These images suggest that as the f/o ratio increases from fuel lean to fuel rich mixtures, the reaction temperature also increases, facilitating the growth of crystallites. Crystallite size and pore size was measured from these TEM micrographs for each f/o ratio studied and are presented in Table IV.

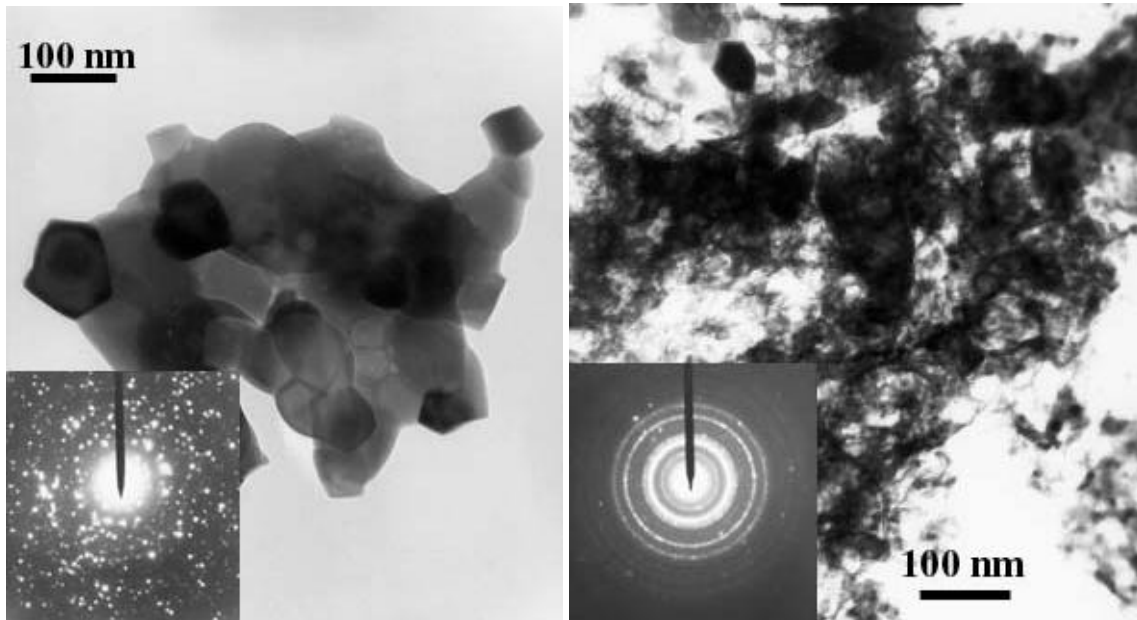


Figure 6. a) Bright field image of well defined crystallites for $f/o = 2.012$ powder. b) Bright field image of a particle that exhibits a "foamy" structure.

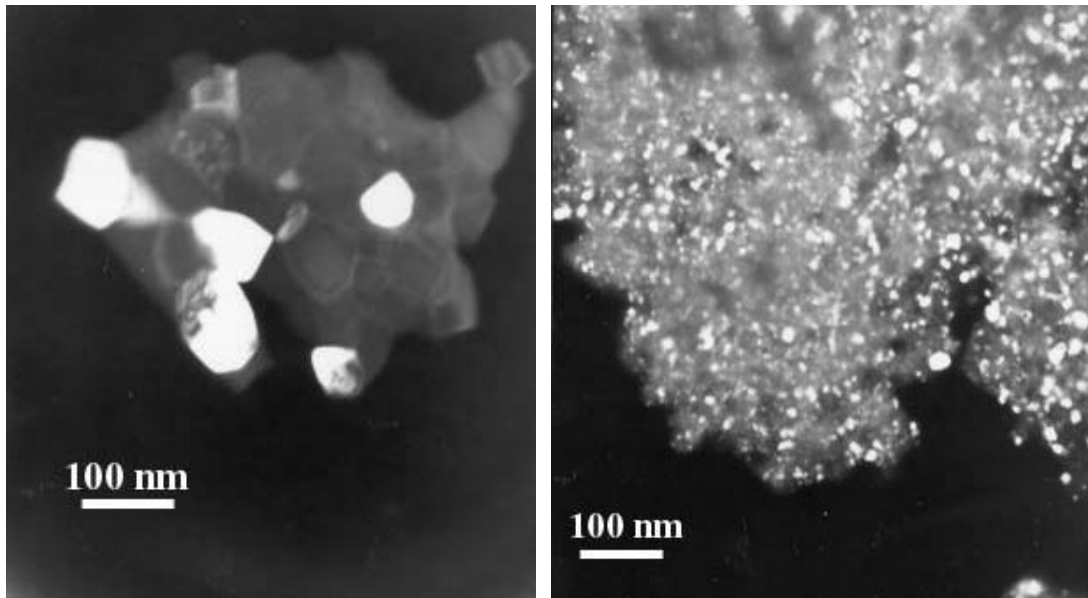


Figure 7. a) Dark field TEM micrograph of $f/o = 2.012$ as-synthesized product showing the crystallites. b) Dark field of a particle with a "foamy" structure from $f/o = 2.012$ powder.

It is believed that the reason why powders produced with a $f/o = 2.012$ exhibit both large and small crystallites is due to the inhomogeneous temperature distribution within the reaction vessel. Particles formed in cooler regions would not exhibit large crystallite sizes since there is not enough heat to grow the crystallites. This explains why the as-synthesized powders must be annealed to transfer all powders to the preferred and more efficient X_2 phase.

Table IV. Measured crystallite and pore size from TEM micrographs.

fuel/oxidizer ratio	Pore size (μm)	Crystallite Size(nm)
0.885	0.03	13
1.250 (Stoich.)	0.03	18
1.615	0.9	36
2.012	1	83

The effect that particle size has on the luminescence intensity was determined by settling annealed powders (1350°C for 1 hour) as described above. Powders were settled for 1, 15, 30, 60 and 120 minutes. Figure 8 shows the particle size distribution determined by laser scattering for each of the settling times.

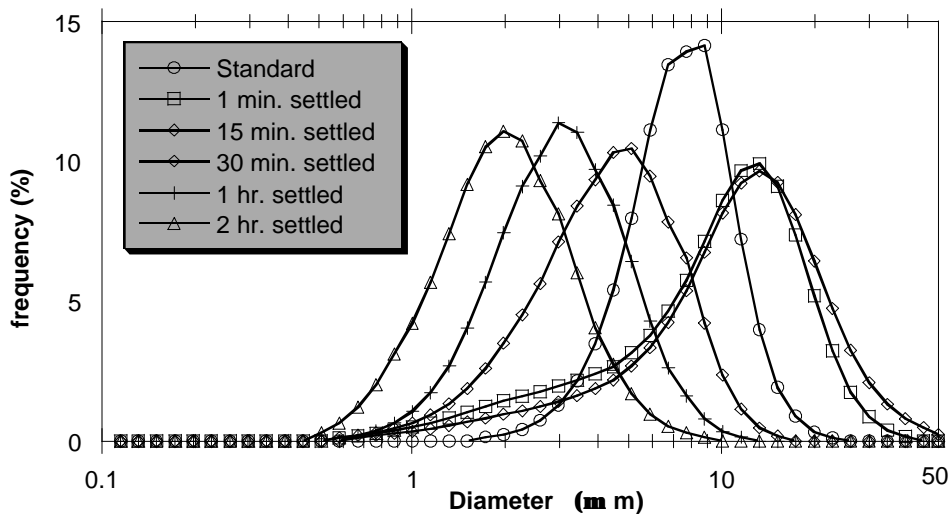


Figure 8. Particle size distribution for settled powders compared to a standard (Nichia).

Figure 8 shows a decrease in the particle size as the settling time is increased beyond 30 minutes. Table V displays the predicted particle size calculated from Eq. [3] and the mean and CV of the particle sizes measured. It is believed that the distribution is broad due to the different sizes and amount of porosity for each particle. Table V shows that the predicted and measured particle sizes are different for the short settling times, but agree well for the longer settling times and again the distribution of the settled particles is broader than that of the standard.

Table V. Predicted particle size diameter as calculated from Eq. [3] compared with the measured mean diameter and coefficient of variation (CV) of the settled particles.

Settling Time (min)	Predicted Dia. (μm)	Mean Dia. Measured (μm)	CV(%)
1	25.5	10.2 ± 6.0	59.0
15	6.6	12.1 ± 7.5	61.9
30	4.7	4.4 ± 2.2	50.5
60	3.3	2.8 ± 1.5	48.9
120	2.3	1.9 ± 1.1	52.1
Standard	--	7.3 ± 2.8	38.2

The effect particle size has on the CL efficiency is shown in Figure 9. The settled powders all have approximately the same CL efficiency, with an average standard deviation over all voltages of 0.035 lm/W. The standard was found to be more efficient over this standard deviation and could be caused by contamination from chlorine (Cl) from the HCl.

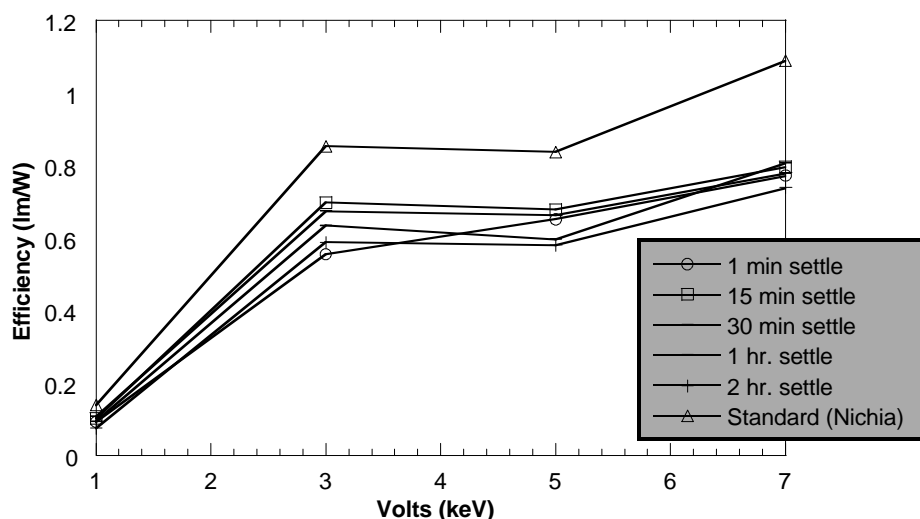


Figure 9. Efficiency of annealed settled powders compared with a standard.

Powders were also milled with an attrition mill using ZrO_2 milling media. Figure 10 shows the CL efficiency of the milled powders as compared with a standard. The unmilled powder was found to have a comparable efficiency compared with the standard at all excitation voltages, while the milled powders were found to have decreasing efficiencies.

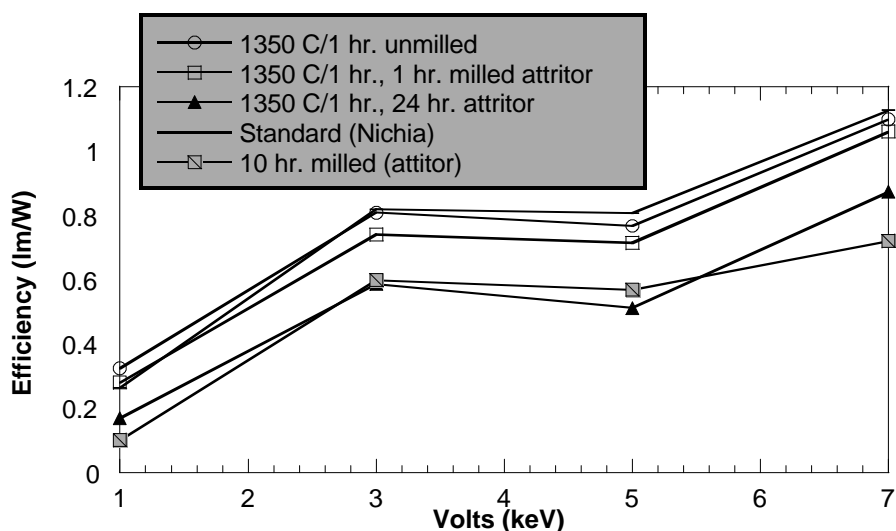


Figure 10. Cathodoluminescence efficiency of milled powders compared with a standard.

CONCLUSIONS

$(Y_{1-m-n}Ce_mGd_n)_2SiO_5$ was produced by combustion synthesis with various f/o ratios. X-ray diffraction analysis on the as-synthesized powders show that as the f/o ratio increase from 0.885 (30% fuel lean) to 2.012 (60% fuel rich), the crystallite size of the powders also increases. At a with f/o = 2.012 both the low temperature X_1 phase and high temperature X_2 phases are present. At lower f/o ratios, only the X_1 phase was observed. Electron diffraction patterns confirmed that the X_1 phase was present in the nanocrystalline, "foam-like" materials. Thermodynamic modeling of the combustion reaction shows that as the f/o ratio increases the amount of gas produced also increases. It was shown that as the amount of fuel increases, the particle size is not affected but the porosity of the particles becomes larger. Bright and dark field transmission electron microscopy micrographs revealed that the crystallite size and average pore size increases with increasing fuel in the combustion synthesis reaction. The cathodoluminescence efficiency of the settled, annealed particles was found to not be affected by the particle size. The cathodoluminescence efficiency of attrition milled powders showed that the milling decreased the cathodoluminescence efficiency, with unmilled powders having an efficiency comparable to a standard.

ACKNOWLEDGMENTS

We would like to thank the National Science Foundation (Grant NSF DMR9626371) and the Defense Advanced Research Projects Agency through the Phosphor Technology Center of Excellence (Grant MDA972-93-1-0030) for supporting this research. Also, we thank Vladimir and Esther Sluzky of Displays Research Laboratories, Inc., San Diego, CA.

REFERENCES

1. R. Simpson, *Videowalls: The book of the Big Electronic Image*, Focal Press, Oxford (1997)
2. Y. Yoshida, A. Ishizuka, and H. Makishima, *Materials Chemistry and Physics* **40**, 267 (1995).
3. J. McKittrick, B. Houghooghi, W. Dubbelday, K. Kavanagh, K. Kinsman, L. Shea, and E. Sluzky in *Scintillator and Phosphor Materials*, P.L. M.J. Weber, R.C. Ruchti, C. Woody, W.M. Yen, R.-y Zhu, Editors, *Mat. Res. Soc. Proc.* **348**, San Francisco, 519-524 (1994).
4. K. Ohno and T. Abe, *J. Electrochem. Soc.* **141**, 1252 (1994).
5. E.J. Bosze, G.A. Hirata, and J. McKittrick, *Society for Information Display*, in press
6. J. J. Kingsley and K. C. Patil, *Mat. Letters* **6**, 427 (1988).
7. E. J. Bosze, G. A. Hirata, J. McKittrick, and L. E. Shea in *Flat-Panel Display Materials-1998*, G.N. Parsons, C.-C. Tsai, T.S. Fahlen, and C.H. Seager, Editors, *Mat. Res. Soc. Proc.* **508**, San Francisco, CA, 269-274 (1998).
8. B.D. Cullity, *Elements of X-ray Diffraction*, Addison-Wesley, Reading, MA (1978)
9. TEQWORKS, "KSG Associates, Inc.," Williamsville, NY 14221.
10. L. Ozawa, *Cathodoluminescence: Theory and Application*, Kodansha Ltd., Tokyo (1990)
11. J. Lin, Q. Su, H. Zhang, and S. Wang, *Mat. Res. Bull.* **31**, 189 (1996).